

A Comprehensive Self-interference Model for Single-antenna Full-duplex Communication Systems

Md Atiqul Islam and Besma Smida
Department of Electrical and Computer Engineering
University of Illinois at Chicago
Chicago, USA
mislam23@uic.edu, smida@uic.edu

Abstract—Single-antenna full-duplex communication technology has the potential to substantially increase spectral efficiency. However, limited propagation domain cancellation of single-antenna system results in a higher impact of receiver chain nonlinearities on the residual self-interference (SI) signal. In this paper, we offer a comprehensive SI model for single-antenna full-duplex systems based on direct-conversion transceiver structure considering nonlinearities of all the transceiver radio frequency (RF) components, in-phase/quadrature (IQ) imbalances, phase noise effect, and receiver noise figure. To validate our model, we also propose a more appropriate digital SI cancellation approach considering receiver chain RF and baseband nonlinearities. The proposed technique employs orthogonalization of the design matrix using QR decomposition to alleviate the estimation and cancellation error. Finally, through circuit-level waveform simulation, the performance of the digital cancellation strategy is investigated, which achieves 20 dB more cancellation compared to existing methods.

Index Terms—Full-duplex, single-antenna, self-interference, digital cancellation, nonlinearity, phase noise, IQ imbalances.

I. INTRODUCTION

Full-duplex technology is one of the emerging techniques to achieve higher spectral efficiency, where devices simultaneously transmit and receive at a single frequency. This novel paradigm in improving spectrum usage can increase the throughput by a factor of two compared to the traditional bi-directional half-duplex, namely time-division duplexing and frequency-division duplexing. However, the implementation of full-duplex systems is constrained by the cancellation of self-interference (SI), which is stemming from the transmitter to the receiver hindering the detection of the received signal.

Recent works [1]–[36] have investigated several different system architectures and cancellation techniques to alleviate the SI in the full-duplex receiver. The SI cancellation techniques can be categorized in a tripartite manner: propagation domain isolation, analog/radio frequency (RF) domain suppression and digital cancellation [1]. The propagation domain isolation or antenna cancellation is accomplished using a combination of antenna directionality [2], path loss [3], cross-polarization [4], and electrical balance isolator network [5]. Suppression in analog domain is achieved by subtracting a processed copy of the transmitted signal from the receiver input [6]–[8]. However, antenna and analog domain suppression are not sufficient to mitigate the strong SI signal below the weak desired signal [1]. Therefore, the residual SI at the detector

input of the receiver chain increases the noise floor, which calls for another cancellation stage in the digital domain.

Digital domain cancellation is accomplished by SI regeneration using digital filters fitted to the detector input through the known transmit data. For digital cancellation techniques, the effect of transmitter and receiver power amplifier (PA) nonlinearities is analyzed in [1], [9], whereas the impact of in-phase/quadrature (IQ) imbalances and resulting image components is investigated in [10]. Signal models including the phase noise of transmitter and receiver oscillators are presented in [11]. It was observed that the phase noise is a bottleneck for perfect SI cancellation while using two different oscillators for transmitter and receiver. A scenario with common oscillator for both the transceiver sides is also analyzed in [12].

In previous literature, both single-antenna and separate-antenna full-duplex models are investigated. However, using single-antenna as a function of SI cancellation is more attractive because of twofold reasons: first, using two antenna full-duplex system may not achieve any higher throughput than using two antenna in half-duplex MIMO system spatially multiplexing two independent packets at the same time [1], [6]; second, using single-antenna transceiver system results in a compact design. Existing single-antenna full-duplex antenna and analog cancellation methods typically achieve 50-60 dB cancellation [5], [13], [14], where separate-antenna system provides higher cancellation. For a practical receiver, this limited RF cancellation results in a higher effect of receiver RF and baseband (BB) nonlinearity on the SI signal.

In this paper, we offer a comprehensive self-interference model for single-antenna full-duplex systems based on direct-conversion structure considering all the impairments including transmitter and receiver IQ imbalances, nonlinear distortions in all the transceiver components, receiver noise figure, and phase noise effect of both transmitter and receiver IQ mixers. Through extensive circuit-level waveform simulation, we show the effect of receiver RF and BB second and third-order nonlinearity on the residual self-interference signal for limited antenna and RF cancellation. To tackle this effect, we propose an appropriate self-interference estimation and digital cancellation approach considering receiver chain nonlinearities, which outperforms the existing digital cancellation techniques. To reduce the estimation and cancellation error, we employ orthogonalization of the design matrix using QR decomposition method.

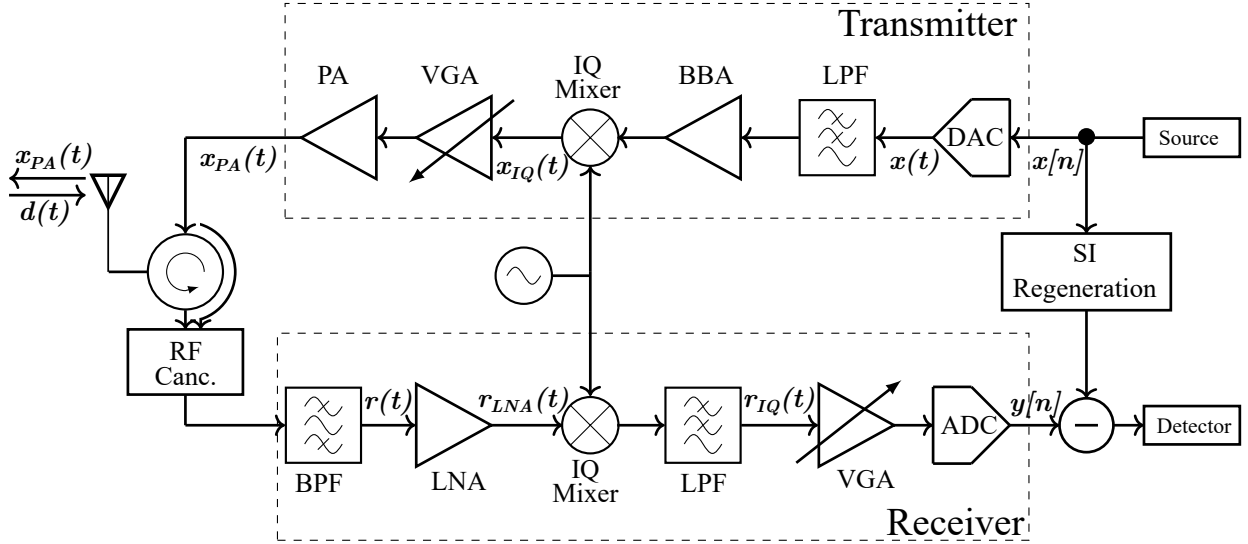


Fig. 1. Detailed block diagram of a single-antenna full-duplex direct conversion transceiver

II. FULL-DUPLEX TRANSCEIVER MODEL AND SELF-INTERFERENCE CHARACTERIZATION

In this section, we discuss the self-interference signal modeling for a single-antenna full-duplex transceiver system based on the direct-conversion structure presented in Fig. 1. In direct-conversion structure, RF and BB signal frequency translation is performed without any intermediate frequency stage unlike superheterodyne structure [37]. The direct-conversion receiver structure allows signal amplification and filtering at the BB stage, which reduces the power consumption and manufacturing cost. However, direct-conversion radios suffer from RF and BB impairments, such as IQ imbalances, nonlinear distortions, and phase noise effect [38]. Therefore, a detailed characterization of the self-interference signal is performed in the next subsections considering the RF and BB impairments.

A. Self-interference Model at the Transmitter

At the transmit chain, the impairments are mainly introduced by the RF front-end components, specifically IQ mixers and power amplifiers. Both baseband and bandpass modeling approach are taken into account for the following SI characterization.

After the digital-to-analog converters (DACs), the I and Q components of the converted baseband signal $x(t)$ are passed through the low-pass filters for further suppression of aliasing products. The I and Q signals are then fed into the IQ mixer for upconversion to the carrier frequency. As stated in [10], IQ imbalances in practical mixers add a mirror image of the original signal with certain image attenuation. The IQ mixers also induce phase noise to the signal. Let γ_{Tx} , λ_{Tx} be the complex gain of the linear and image signal components, respectively. Thus, the upconverted RF signal is given by

$$\begin{aligned} x_{IQ}(t) &\doteq 2\Re\left\{\left(\gamma_{Tx} x(t) + \lambda_{Tx} \bar{x}(t)\right)e^{j(\omega_c t + \theta_{Tx})}\right\} \\ &= z(t)e^{j(\omega_c t + \theta_{Tx})} + \bar{z}(t)e^{-j(\omega_c t + \theta_{Tx})}, \end{aligned} \quad (1)$$

where $z(t) = (\gamma_{Tx} x(t) + \lambda_{Tx} \bar{x}(t))$, ω_c is the angular center frequency of the RF signal and $\theta_{Tx}(t)$ is the random phase noise process. Here, $(\bar{\cdot})$ denotes the complex conjugate.

Before transmission, the upconverted signal goes through variable amplification stages (variable gain amplifier (VGA), PA driver) to meet the transmit power specifications. Then, for final amplification, the signal is fed into the power amplifier operating in its nonlinear region. Only the odd-order nonlinear terms are considered for PA, as the even-power harmonics lie out of band and will be cutoff by the RF low pass filter (LPF) of the receiver [10] [1]. Considering the VGA gain as β_{VGA} , the PA nonlinear response is modeled based on the Hammerstein nonlinearity, given as

$$x_{PA}(t) \doteq \left(\sum_{p \in \{1,3\}} \beta_{PA,p} (\beta_{VGA} x_{IQ}(t))^p \right) * f(t), \quad (2)$$

where p is the order of the nonlinearity, $f(t)$ is the memory polynomial, and $(*)$ denotes the linear convolution. Here, $\beta_{PA,1}$ is the linear gain and $\beta_{PA,3}$ is the gain of third-order nonlinear distortions. We consider only up to the third-order distortion, as that is in practice always the strongest nonlinearity at PA output [10]. A general definition of the nonlinear distortion gains is given as

$$\beta_{C,n} \doteq \frac{\beta_{C,1}}{(IIP_n)^{n-1}}, \quad (3)$$

where $\beta_{C,1}$ denotes the linear gain and n is the nonlinearity order of any component $C = \{PA, LNA, BB\}$. These nonlinear distortions are modeled using IIP2 and IIP3 figures (second and third order input-referred intercept points) of the PA [37].

In single-antenna system, the PA output is routed to the antenna using a circulator. In addition to routing signals between the transceiver and antenna, the circulator should also provide a very high isolation between the transmitter (Tx) and receiver (Rx). Unfortunately, practical circulators provide only

about 15–20 dB isolation contributing to a direct path between Tx and Rx as circulator leakage [1]. There is another path of SI due to the antenna reflection [7]. Because of the mismatch between transmitter line impedance and antenna impedance, a portion of the transmitted signal reflects back to the receiver front end. While these two signals are considered to be the main coupling components of the SI, there are also weaker multipath components due to the reflections from surrounding environment. At the receiver input, the SI signal subjects to the RF cancellation. Letting $\alpha_{RF}(t)$, $h_{ch}(t)$ be the impulse response of the RF cancellation and the multipath channel respectively, the signal at the receiver input is given by

$$r(t) \doteq \alpha_{RF}(t) * h_{ch}(t) * x_{PA}(t) + d(t) + \eta_{th}(t) \quad (4)$$

$$\stackrel{(a)}{=} \sum_{p \in \{1,3\}} h_p(t) * (x_{IQ}(t))^p + d(t) + \eta_{th}(t),$$

where $h_p(t) = \beta_{PA,p} \beta_{VGA}^p (\alpha_{RF}(t) * f(t) * h_{ch}(t))$ and $d(t)$, η_{th} are the desired signal and the thermal noise of the receiver, respectively. Here, (a) is defined using (2).

B. Self-interference Model at the Receiver

As a direct-conversion receiver suffers from Low Noise Amplifier (LNA) nonlinearities, Mixer IQ imbalance, and BB nonlinearity, these impairments will have a significant effect on the self-interference signal, especially in higher transmit power case. Therefore, a detailed receiver chain SI modeling is performed considering all the receiver impairments.

At the first stage of the receiver, the signal is amplified by a nonlinear LNA. We model the LNA using the same Hammerstein model used in (3). The LNA output is given by

$$r_{LNA}(t) \doteq \sum_{q \in \{1,3\}} \beta_{LNA,q} (r(t))^q + \eta_{LNA}(t)$$

$$\stackrel{(b)}{=} \sum_{q \in \{1,3\}} \beta_{LNA,q} \left(\sum_{p \in \{1,3\}} h_p(t) * (x_{IQ}(t))^p + d(t) + \eta_{th}(t) \right)^q + \eta_{LNA}(t)$$

$$\approx \sum_{q \in \{1,3\}} \beta_{LNA,q} \left(\sum_{p \in \{1,3\}} h_p(t) * (x_{IQ}(t))^p \right)^q + c(t), \quad (5)$$

where $\eta_{LNA}(t)$ is the noise of the LNA and q is the order of the nonlinearity. Here, (b) is defined using (4). For brevity, we only consider the linear operation of the receiver components for the desired signal and noise. Therefore, $c(t) = \beta_{LNA,1} (d(t) + \eta_{th}(t)) + \eta_{LNA}(t)$. Here, $\beta_{LNA,1}$ and $\beta_{LNA,q}$ are the linear gain and respective q th order nonlinear distortion gain of the LNA. Only odd order distortions are considered, as the even order RF LNA nonlinearities produce frequency components that are far away from ω_c and will be filtered out by low pass filter (LPF) [37], [38].

After the LNA, receiver IQ mixer downconverts the RF signal into baseband frequency and LPFs are used to filter out the high frequency terms. Practical IQ mixers induce random

phase noise $\theta_{Rx}(t)$, which is uncorrelated to $\theta_{Tx}(t)$ in case of independent oscillators [19]. However, in single-antenna full-duplex system, same oscillator is shared by the transmitter and the receiver resulting in a common phase noise process, $\theta(t)$. Thus, $\theta_{Tx}(t) = \theta_{Rx}(t) = \theta(t)$. It is shown in previous literature that sharing oscillators suppresses the phase noise below the noise floor even in the case of transmission delay [12], [19]. So, the downconverted signal is written as

$$r_{IQ}(t) \doteq \text{LPF} \left\{ r_{LNA}(t) e^{-j(\omega_c t + \theta_{Rx}(t))} \right\}$$

$$= \text{LPF} \left\{ \left(\sum_{q \in \{1,3\}} \beta_{LNA,q} \left(\sum_{p \in \{1,3\}} h_p(t) * (x_{IQ}(t))^p \right)^q + c(t) \right) e^{-j(\omega_c t + \theta_{Rx}(t))} \right\}$$

$$= \text{LPF} \left\{ \sum_{q \in \{1,3\}} \beta_{LNA,q} \left(\sum_{p \in \{1,3\}} h_p(t) * (z(t) e^{j(\omega_c t + \theta_{Rx}(t))} + \bar{z}(t) e^{-j(\omega_c t + \theta_{Rx}(t))})^p \right)^q e^{-j(\omega_c t + \theta_{Rx}(t))} \right\} + c(t)$$

$$= \sum_{q \in \{1,3\}} \beta_{LNA,q} \left(\frac{q}{\frac{q-1}{2}} \right) (h_1(t) * z(t) + h_3(t) * 3z^2(t) \bar{z}(t))^{\frac{q+1}{2}}$$

$$\left(h_1(t) * \bar{z}(t) + h_3(t) * 3z(t) \bar{z}(t)^2 \right)^{\frac{q-1}{2}} + c(t)$$

$$= \sum_{q \in \{1,3\}} \beta_{LNA,q} \left(\frac{q}{\frac{q-1}{2}} \right) \left(\sum_{p \in \{1,3\}} h_p(t) * u_p(t) \right)^{\frac{q+1}{2}}$$

$$\left(\sum_{p \in \{1,3\}} h_p(t) * \bar{u}_p(t) \right)^{\frac{q-1}{2}} + c(t)$$

$$= s_{IQ}(t) + c(t), \quad (6)$$

where

$$s_{IQ}(t) = \sum_{q \in \{1,3\}} \beta_{LNA,q} \left(\frac{q}{\frac{q-1}{2}} \right) \left(\sum_{p \in \{1,3\}} h_p(t) * u_p(t) \right)^{\frac{q+1}{2}}$$

$$\left(\sum_{p \in \{1,3\}} h_p(t) * \bar{u}_p(t) \right)^{\frac{q-1}{2}}$$

$$u_1(t) = \gamma_{Tx} x(t) + \lambda_{Tx} \bar{x}(t)$$

$$u_3(t) = 3 \left(\gamma_{Tx}^2 \bar{\lambda}_{Tx} x^3(t) + (\gamma_{Tx}^2 \bar{\gamma}_{Tx} + 2\gamma_{Tx} \lambda_{Tx} \bar{\lambda}_{Tx}) x^2(t) \bar{x}(t) \right. \\ \left. + (2\gamma_{Tx} \bar{\gamma}_{Tx} \lambda_{Tx} + \lambda_{Tx}^2 \bar{\lambda}_{Tx}) x(t) \bar{x}^2(t) + \lambda_{Tx}^2 \bar{\gamma}_{Tx} \bar{x}^3(t) \right). \quad (7)$$

The reader is referred to the Appendix for necessary proofs of (6). Receiver IQ mixer also induces the image component because of the IQ imbalance. Now, considering the effect of IQ imbalance, the IQ output signal is written as

$$r_{IQIm}(t) \doteq \gamma_{Rx} r_{IQ}(t) + \lambda_{Rx} \bar{r}_{IQ}(t) + \eta_{IQ}(t), \quad (8)$$

where γ_{Rx} , λ_{Rx} are the linear and image component gain, and $\eta_{IQ}(t)$ is the noise of the IQ mixer.

Baseband components shown in Fig. 1, specifically amplifiers and analog-to-digital converters (ADCs) also introduce some nonlinearities and DC offset to the BB signal. For simplification, up to second order nonlinearity is considered.

In our model, we use the complex representation of the baseband signal since it helps analytically by revealing how the distortion components are spectrally distributed in relation to the original signal. Considering all the impairments, the complex baseband signal is written as

$$r_{BB}(t) \doteq \sum_{m=0}^2 \beta_{BB,r} r_{IQIm}^m(t) + \eta_{BB}(t), \quad (9)$$

where m is the order of the nonlinearity, $\beta_{BB,r}$ and $\eta_{BB}(t)$ is the respective m th order baseband gain and the BB components noise, respectively. The first term of (9) represents the DC offset introduced by the baseband components. At the end of the receiver chain, the ADC converts the analog baseband signal to digital domain. Considering the quantization noise, $n_{quant}[n]$ induced by the ADC, the digital signal at the ADC output is expressed as

$$\begin{aligned} y[n] &\doteq r_{BB}[n] + \eta_{Quant}[n] \\ &= \sum_{m=0}^2 \beta_{BB,r} \left(\gamma_{Rx} s_{IQ}[n] + \lambda_{Rx} \bar{s}_{IQ}[n] \right)^m \\ &\quad + \beta_{BB,1} \gamma_{Rx} \beta_{LNA,1} d[n] + \eta_T[n]. \end{aligned} \quad (10)$$

Here, $\eta_T[n]$ represents the total noise of the receiver including thermal noise, receiver noise figure and quantization noise.

III. PROPOSED DIGITAL ESTIMATION AND CANCELLATION OF SELF-INTERFERENCE SIGNAL

In this section, we propose an appropriate digital cancellation approach with improved reference signal design for estimation based on the signal at the ADC output. To ensure the estimation accuracy, orthogonalization procedure is employed in estimation technique.

Based on (10) and (7), $y[n]$ can be expressed as the combination of the linear SI signal $x[n]$, conjugate SI signal $\bar{x}[n]$, and their higher order terms along with desired signal, and receiver noise floor. Although a detailed expansion of (10) results in hundreds of residual SI terms, most of the higher order terms are very weak. Therefore, they have insignificant effect on the total self-interference power, thus can be ignored

without compromising self-interference cancellation accuracy. Based on the specification in Table II, we keep the 13 stronger SI components that include combination of $x[n]$, $\bar{x}[n]$, and their higher order terms and use those for cancellation of the self-interference signal. Hence, using vector matrix notation, for N observed training samples, the ADC output signal is written as

$$\mathbf{Y} = \mathbf{\Psi} \mathbf{w} + \mathbf{d} + \boldsymbol{\eta}, \quad (11)$$

where $\mathbf{Y} = [y[n] \ y[n+1] \ \dots \ y[n+N-1]]^T$, $\mathbf{d} = [\beta_{BB,1} \gamma_{Rx} \beta_{LNA,1} [d[n] \ d[n+1] \ \dots \ d[n+N-1]]^T$, and $\boldsymbol{\eta} = [\eta_T[n] \ \eta_T[n+1] \ \dots \ \eta_T[n+N-1]]^T$. The definition of the design matrix $\mathbf{\Psi}$ with size $N \times (2L + 3L^2 + 7L^3 + 1)$ are given in (12), where L is the length of the total impulse response including multipath channel, analog cancellation, and PA memory polynomial. Here, the horizontally concatenated basis matrices represent the 13 stronger SI terms formulated using (13) and (14). For instance, the matrix $\mathbf{\Psi}_{x,\bar{x},x^2\bar{x}} \in \mathbb{C}^{N \times L^3}$ represent the SI term: $9\beta_{BB,1} \gamma_{Tx} \beta_{LNA,3} \gamma_{Rx} \bar{\gamma}_{Tx} (\gamma_{Tx}^2 \bar{\gamma}_{Tx} + 2\gamma_{Tx} \lambda_{Tx} \bar{\lambda}_{Tx}) (h_1[n] * x[n]) (h_1[n] * \bar{x}[n]) (h_3[n] * x^2[n] \bar{x}[n])$.

Here, \mathbf{w} is the $(2L + 3L^2 + 7L^3 + 1) \times 1$ parameter vector. Our goal is to estimate the parameter \mathbf{w} , and then use it to reconstruct and cancel the self-interference signal at the detector input. Therefore, the error vector is defined as

$$\mathbf{e} = \mathbf{Y} - \mathbf{\Psi} \hat{\mathbf{w}}, \quad (15)$$

where $\hat{\mathbf{w}}$ is the least square estimate, which can be obtained by solving for the \mathbf{w} that minimizes the power of the error vector as

$$\hat{\mathbf{w}} = \arg \min_{\mathbf{w}} \|\mathbf{e}\|^2 = \arg \min_{\mathbf{w}} \|\mathbf{Y} - \mathbf{\Psi} \mathbf{w}\|^2. \quad (16)$$

The above ordinary least square problem has closed form solution with the usual assumption that the design matrix $\mathbf{\Psi}$ has independent columns. However, the columns of the matrix $\mathbf{\Psi}$ are higher order polynomials of linear SI component $x[n]$, conjugate SI component $\bar{x}[n]$, and their interaction products. Therefore, the columns of the matrix $\mathbf{\Psi}$ are correlated, thus

$$\mathbf{\Psi} = [\mathbf{1} \ \mathbf{\Psi}_x \ \mathbf{\Psi}_{\bar{x}} \ \mathbf{\Psi}_{x,x} \ \mathbf{\Psi}_{x,\bar{x}} \ \mathbf{\Psi}_{\bar{x},\bar{x}} \ \mathbf{\Psi}_{x,x,x} \ \mathbf{\Psi}_{x,x,\bar{x}} \ \mathbf{\Psi}_{x,\bar{x},\bar{x}} \ \mathbf{\Psi}_{\bar{x},\bar{x},\bar{x}} \ \mathbf{\Psi}_{x,x,x^2\bar{x}} \ \mathbf{\Psi}_{x,\bar{x},x^2\bar{x}} \ \mathbf{\Psi}_{x,x,x\bar{x}^2}], \quad (12)$$

where $\mathbf{1}$ denotes an $N \times 1$ column vector with all ones. Letting $\mathbf{a}, \mathbf{b}, \mathbf{c} \in \{x, \bar{x}, x^2\bar{x}, x\bar{x}^2\}$, each of the horizontally concatenated matrices of $\mathbf{\Psi}$ can be formulated as

$$\begin{aligned} \mathbf{\Psi}_a &= [\Phi_a(n) \ \Phi_a(n-1) \ \dots \ \Phi_a(n-L+1)] \\ \mathbf{\Psi}_{a,b} &= [\Phi_b(n) \odot \mathbf{\Psi}_a \ \Phi_b(n-1) \odot \mathbf{\Psi}_a \ \dots \ \Phi_b(n-L+1) \odot \mathbf{\Psi}_a] \\ \mathbf{\Psi}_{a,b,c} &= [\Phi_c(n) \odot \mathbf{\Psi}_{a,b} \ \Phi_c(n-1) \odot \mathbf{\Psi}_{a,b} \ \dots \ \Phi_c(n-L+1) \odot \mathbf{\Psi}_{a,b}], \end{aligned} \quad (13)$$

where \odot denotes element wise multiplication of the vector with all the columns of the matrix. Here, the basis vectors are defined as

$$\begin{aligned} \Phi_x(n) &= [x[n] \ x[n+1] \ \dots \ x[n+N-1]]^T, & \Phi_{\bar{x}}(n) &= \bar{\Phi}_x(n), \\ \Phi_{x^2\bar{x}}(n) &= [x^2[n] \bar{x}[n] \ x^2[n+1] \bar{x}[n+1] \ \dots \ x^2[n+N-1] \bar{x}[n+N-1]]^T, & \Phi_{x\bar{x}^2}(n) &= \bar{\Phi}_{x^2\bar{x}}(n). \end{aligned} \quad (14)$$

TABLE I
WAVEFORM AND SYSTEM LEVEL PARAMETERS

Parameter	Value	Parameter	Value
Bandwidth	20 MHz	SNR Requirement	10 dB
Carrier Frequency	2.4 GHz	Thermal Noise Floor	-101.0 dBm
Constellation	16-QAM	RX Noise Figure	4.1 dB
Number of Subcarriers	64	Sensitivity Level	-86 dBm
Cyclic Prefix Length	16	Transmit Power	-5:25 dBm
Sample length	15.625 ns	ADC Bits	12
Symbol Length	4 μ s	PAPR	10 dB

TABLE II
FULL-DUPLEX TRANSCIVER COMPONENT PARAMETERS

Parameter	Value	Parameter	Value
PA Gain	27 dB	LNA Gain	20 dB
PA IIP3	13 dBm	LNA IIP3	-3 dBm
VGA (Tx) Gain	0:33 dB	BB IIP2	50 dBm
IRR (Tx)	30 dB	IRR (Rx)	30 dB

there exists high level of multicollinearity. To tackle this problem, we propose to orthogonalize the design matrix Ψ using QR decomposition. We use traditional Gram-Schmidt orthogonalization procedure to find a QR decomposition of Ψ such that $\Psi = \mathbf{QR}$, where \mathbf{Q} has orthogonal columns and same rank as Ψ . Here, \mathbf{R} is an upper triangular matrix with 1 on the diagonal. Using the QR decomposition, (16) is written as

$$\hat{\mathbf{w}} = \arg \min_w \|\mathbf{Y} - \mathbf{QR}\mathbf{w}\|^2. \quad (17)$$

Letting $\boldsymbol{\mu} = \mathbf{R}\mathbf{w}$, we can reformulate the above minimization problem and find the least square solution as

$$\begin{aligned} \hat{\boldsymbol{\mu}} &= \arg \min_{\boldsymbol{\mu}} \|\mathbf{Y} - \mathbf{Q}\boldsymbol{\mu}\|^2 \\ &= (\mathbf{Q}^H\mathbf{Q})^{-1}\mathbf{Q}^H\mathbf{Y}, \end{aligned} \quad (18)$$

where $(\cdot)^H$ denotes the Hermitian transpose of the matrix. Using back substitution, we derive $\hat{\mathbf{w}}$ from $\hat{\boldsymbol{\mu}}$.

It is to be noted that authors in [10] proposed a widely linear canceller considering only the effect of linear SI $x[n]$ and conjugate SI $\bar{x}[n]$, a nonlinear approach considering third order nonlinear SI term $x^2[n]\bar{x}[n]$ is provided in [1], and a joint cancellation technique cascading PA nonlinearity with transmitter IQ imbalance is proposed in [18] for MIMO cases, which is converted here into single antenna system. However, receiver nonlinearities and its effect are ignored in these previous models. Our proposed estimation approach takes these components into account for the formulation of the design matrix and provides required SI cancellation at the detector input.

IV. PERFORMANCE SIMULATION AND ANALYSIS

In this section, we perform a waveform simulation to evaluate the performance of the proposed digital cancellation strategy and compare with the previous methods.

A. Simulation Parameters

The transceiver architecture provided in Fig. 1 is followed explicitly to perform the waveform simulation. The simulator

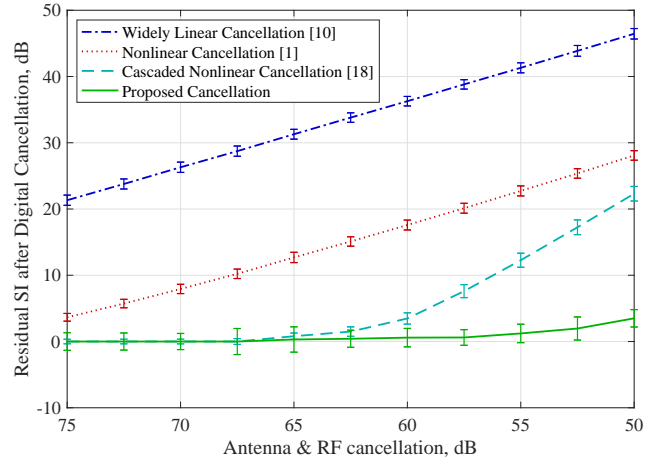


Fig. 2. Residual self-interference power after digital cancellation with respect to different RF cancellation value and 25 dBm transmit Power

is implemented using MATLAB baseband equivalent model of the components, which includes the impact of all the transceiver impairments. The waveform simulation is based on a 20 MHz OFDM-based system with 64 subcarriers per OFDM symbols as in IEEE802.11 systems. The additional parameters of the waveforms are shown in Table I. The system level component parameters of the full-duplex transceiver are provided in Table II, which are taken from the datasheet of AD9361 transceiver made by Analog Devices [39]. We perform our simulation based on single-antenna full-duplex system with a circulator providing a stronger leakage signal to the receiver as the direct SI component and several multipath components [5]. Therefore, the SI channel is simulated as a Rician channel with a K-factor of 30 dB and 4 non-line-of-sight (nLOS) components each delayed by one sample [25]. To emulate IEEE802.11 system, we use WLAN packet formatting where each packet consists of 120 OFDM symbols. Around 8% of the total packet size are considered as training symbols, which are used to estimate and cancel the self-interference. We use 1000 Monte Carlo simulation runs to calculate the average cancellation performance. Here, we consider 15dB circulator isolation with variable RF cancellation values to show its impact on the digital cancellation.

B. SI Cancellation Capability and SINR

First, for variable antenna and RF cancellation, we compare the performance of the proposed digital cancellation technique with previous methods. In Fig. 2, we represent the residual self-interference signal strength of several digital cancellation methods from the measured noise floor with respect to 50-75 dB antenna and RF cancellation for a transmit power of 25 dBm. We also include the error bars at one standard deviation from the mean of the cancellation value. We observe that widely linear cancellation [10] scheme has a residual of 20-45 dB. Although considering the nonlinear cancellation [1] along with linear and widely linear methods increases the performance drastically, it has a residual of around 30 dB at an antenna and RF cancellation of 50 dB. For higher antenna

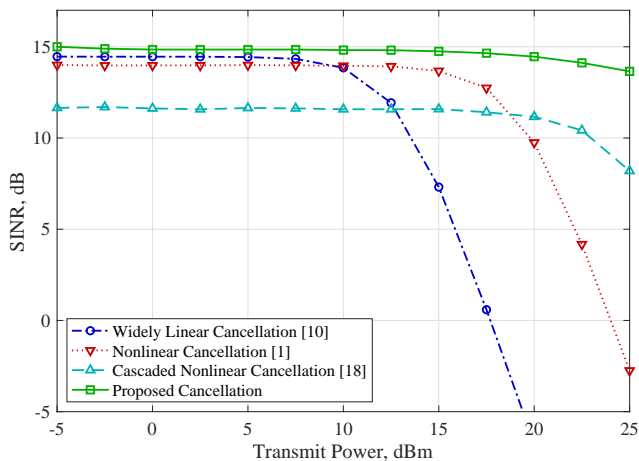


Fig. 3. The SINRs for different digital cancellation method with respect to the overall transmit power with antenna and RF cancellation of 60 dB

and RF suppression, cascaded cancellation [18] performance is comparable with our proposed method. However, below 65 dB cancellation, it has a sharp growth of the residual leading almost 22 dB for 50 dB antenna and RF cancellation. In comparison with these methods, our proposed digital cancellation technique provides better performance contributing only around 3 dB residual at a very low RF cancellation. This performance boost is because of the inclusion of receiver chain second and third-order nonlinearities in our proposed method, whereas all the previous methods took only the transmitter PA nonlinearities into account ignoring the receiver chain nonlinear distortions. However, that assumption provides comparable performance in case of high antenna and RF cancellation or linear receiver operation. As we observed, for practical transceivers such as AD9361, the receiver performance is not linear. Therefore, limited antenna and RF cancellation, typically below 65 dB, results in the higher self-interference signal power at the receiver input, which contributes to a stronger nonlinear effect of the receiver chain components. In this scenario, the proposed digital cancellation strategy outperforms the previous techniques.

In Fig. 3, we show the performance of the digital cancellation methods with respect to the transmit power varying from -5 dBm to 25 dBm while considering 60 dB antenna and RF cancellation. Here, signal-to-interference-plus-noise-ratio (SINR) is used as the figure-of-merit of the cancellation strategies. During calculation of the SINR, the desired signal is naturally present with an SNR of 15 dB, which is the maximum achievable SINR. From Fig. 3, we observed that our proposed method outperforms the previous techniques for all the transmit power cases. Nonlinear [1] and widely linear [10] methods sufficiently suppress the SI up to the transmit power of 15 and 10 dBm, respectively. Although, the cascaded cancellation [18] method performs better than the previous methods for higher transmit power cases, it suffers from overfitting problem resulting in higher estimation error in low transmit power cases. In our proposed model, we

tackle this problem through orthogonalization of the design matrix, which reduces the estimation error. Thus, our proposed digital cancellation approach provides reliable and sufficient suppression of self-interference signal in a practical nonlinear receiver for a varying antenna and RF cancellation as low as 50 dB.

V. CONCLUSION

The performance of self-interference cancellation in single-antenna full-duplex systems is limited by the presence of hardware impairments in the transceiver chain. In this paper, we provided a detailed modeling of the self-interference signal considering transmitter PA nonlinearities, receiver chain second and third-order nonlinearities, DC offset, IQ imbalances, phase noise, and receiver noise figure. To validate the self-interference model, we proposed a digital cancellation approach considering receiver chain second and third-order nonlinearities and implemented a practical waveform simulator. Our comprehensive simulation showed that, in practical receiver, these nonlinearities have significant effect on the self-interference signal for an analog and RF cancellation of 65 dB or below. In this scenario, our proposed digital cancellation technique outperforms the existing cancellation methods by achieving up to 20 dB more self-interference cancellation. For future work, we intend to extend the self-interference modeling and cancellation for MIMO system considering all the practical transceiver impairments and provide an efficient digital self-interference cancellation strategy.

APPENDIX

Necessary proofs for (9) are provided here.

Let $\omega_c t + \theta_{Rx}(t) = \omega_c t + \theta_{Tx}(t) = \Delta(t)$ as $\theta_{Rx}(t) = \theta_{Tx}(t)$. Now,

$$\begin{aligned}
 & \text{LPF} \left\{ \left(\sum_{q=1,3} \beta_{LNA,q} \left(\sum_{p=1,3} h_p(t) * (x_{IQ}(t))^p \right)^q + c(t) \right) e^{-j\Delta(t)} \right\} \\
 &= \text{LPF} \left\{ \sum_{q=1,3} \beta_{LNA,q} \left((h_1(t) * z(t) + h_3(t) * 3z^2(t)\bar{z}(t)) e^{j\Delta(t)} \right. \right. \\
 &\quad \left. \left. + (h_1(t) * \bar{z}(t) + h_3(t) * 3z(t)\bar{z}(t)^2) e^{-j\Delta(t)} \right)^q e^{-j\Delta(t)} \right\} \\
 &= \text{LPF} \left\{ \sum_{q=1,3} \beta_{LNA,q} \sum_{k=0}^q \binom{q}{k} (h_1(t) * z(t) + h_3(t) * 3z^2(t)\bar{z}(t))^{q-k} \right. \\
 &\quad \left. (h_1(t) * \bar{z}(t) + h_3(t) * 3z(t)\bar{z}(t)^2)^k e^{j\Delta(t)(q-2k-1)} \right\} \\
 &\stackrel{(c)}{=} \sum_{q=1,3} \beta_{LNA,q} \left(\frac{q-1}{2} \right) (h_1(t) * z(t) + h_3(t) * 3z^2(t)\bar{z}(t))^{\frac{q+1}{2}} \\
 &\quad (h_1(t) * \bar{z}(t) + h_3(t) * 3z(t)\bar{z}(t)^2)^{\frac{q-1}{2}}. \tag{19}
 \end{aligned}$$

Here, (c) is achieved if

$$q - 2k - 1 = 0 \Rightarrow k = \frac{q-1}{2}. \tag{20}$$

ACKNOWLEDGMENTS

This work was partially funded by the National Science Foundation CAREER award #1620902.

REFERENCES

- [1] D. Bharadia, E. McMillin, and S. Katti, "Full duplex radios," *ACM SIGCOMM Computer Communication Review*, vol. 43, no. 4, pp. 375–386, 2013.
- [2] J. I. Choi, M. Jain, K. Srinivasan, P. Levis, and S. Katti, "Achieving single channel, full duplex wireless communication," in *Proceedings of International Conference on Mobile Computing and Networking*. ACM, 2010, pp. 1–12.
- [3] D. Korpi, M. Heino, C. Icheln, K. Haneda, and M. Valkama, "Compact inband full-duplex relays with beyond 100 dB self-interference suppression: Enabling techniques and field measurements," *IEEE Transactions on Antennas and Propagation*, vol. 65, no. 2, pp. 960–965, 2017.
- [4] M. E. Knox, "Single antenna full duplex communications using a common carrier," in *IEEE Wireless and microwave technology conference (WAMICON)*. IEEE, 2012, pp. 1–6.
- [5] B. Debaille, D.-J. van den Broek, C. Lavin, B. van Liempd, E. A. Klumperink, C. Palacios, J. Craninckx, B. Nauta, and A. Pärssinen, "Analog/RF solutions enabling compact full-duplex radios," *IEEE Journal on Selected Areas in Communications*, vol. 32, no. 9, p. 1662, 2014.
- [6] M. Jain, J. I. Choi, T. Kim, D. Bharadia, S. Seth, K. Srinivasan, P. Levis, S. Katti, and P. Sinha, "Practical, real-time, full duplex wireless," in *Proceedings of International Conference on Mobile Computing and Networking*. ACM, 2011, pp. 301–312.
- [7] S. Khaledian, F. Farzami, B. Smida, and D. Erricolo, "Inherent self-interference cancellation for in-band full-duplex single-antenna systems," *IEEE Transactions on Microwave Theory and Techniques*, vol. 66, no. 6, pp. 2842–2850, 2018.
- [8] G. C. Alexandropoulos and M. Duarte, "Joint design of multi-tap analog cancellation and digital beamforming for reduced complexity full duplex MIMO systems," in *Proc. IEEE ICC*, Paris, France, May 2017, pp. 1–7.
- [9] E. Ahmed and A. M. Eltawil, "All-digital self-interference cancellation technique for full-duplex systems," *IEEE Transactions on Wireless Communications*, vol. 14, no. 7, pp. 3519–3532, 2015.
- [10] D. Korpi, L. Anttila, V. Syrjälä, and M. Valkama, "Widely linear digital self-interference cancellation in direct-conversion full-duplex transceiver," *IEEE Journal on Selected Areas in Communications*, vol. 32, no. 9, pp. 1674–1687, 2014.
- [11] X. Quan, Y. Liu, S. Shao, C. Huang, and Y. Tang, "Impacts of phase noise on digital self-interference cancellation in full-duplex communications," *IEEE Transactions on Signal Processing*, vol. 65, no. 7, pp. 1881–1893, 2017.
- [12] A. Balatsoukas-Stimming, A. C. Austin, P. Belanovic, and A. Burg, "Baseband and RF hardware impairments in full-duplex wireless systems: experimental characterisation and suppression," *EURASIP Journal on Wireless Communications and Networking*, vol. 2015, no. 1, p. 142, 2015.
- [13] D. Korpi, Y.-S. Choi, T. Huusari, L. Anttila, S. Talwar, and M. Valkama, "Adaptive nonlinear digital self-interference cancellation for mobile inband full-duplex radio: Algorithms and RF measurements," in *IEEE Global Communications Conference (GLOBECOM)*. IEEE, 2015.
- [14] S. Khaledian, F. Farzami, B. Smida, and D. Erricolo, "Robust self-interference cancellation for microstrip antennas by means of phase reconfigurable coupler," *IEEE Transactions on Antennas and Propagation*, vol. 66, no. 10, pp. 5574–5579, 2018.
- [15] A. Sabharwal, P. Schniter, D. Guo, D. W. Bliss, S. Rangarajan, and R. Wichman, "In-band full-duplex wireless: Challenges and opportunities," *IEEE Journal on Selected Areas in Communications*, vol. 32, no. 9, pp. 1637–1652, 2014.
- [16] B. Smida and S. Khaledian, "ReflectFX: In-band full-duplex wireless communication by means of reflected power," *IEEE Transactions on Communications*, vol. 65, no. 5, pp. 2207–2219, 2017.
- [17] D. Korpi, T. Riihonen, V. Syrjälä, L. Anttila, M. Valkama, and R. Wichman, "Full-duplex transceiver system calculations: Analysis of ADC and linearity challenges," *IEEE Transactions on Wireless Communications*, vol. 13, no. 7, pp. 3821–3836, 2014.
- [18] L. Anttila, D. Korpi, E. Antonio-Rodríguez, R. Wichman, and M. Valkama, "Modeling and efficient cancellation of nonlinear self-interference in MIMO full-duplex transceivers," in *IEEE Globecom Workshops (GC Wkshps)*. IEEE, 2014, pp. 777–783.
- [19] A. Sahai, G. Patel, C. Dick, and A. Sabharwal, "On the impact of phase noise on active cancellation in wireless full-duplex," *IEEE transactions on Vehicular Technology*, vol. 62, no. 9, pp. 4494–4510, 2013.
- [20] A. Kiayani, M. Z. Waheed, L. Anttila, M. Abdelaziz, D. Korpi, V. Syrjälä, M. Kosunen, K. Stadius, J. Ryyänen, and M. Valkama, "Adaptive nonlinear RF cancellation for improved isolation in simultaneous transmit–receive systems," *IEEE Transactions on Microwave Theory and Techniques*, vol. 66, no. 5, pp. 2299–2312, 2018.
- [21] D. Korpi, L. Anttila, and M. Valkama, "Feasibility of in-band full-duplex radio transceivers with imperfect RF components: analysis and enhanced cancellation algorithms," in *9th International Conference on Cognitive Radio Oriented Wireless Networks and Communications (CROWNCOM)*. IEEE, 2014, pp. 532–538.
- [22] S. Khaledian, F. Farzami, B. Smida, and D. Erricolo, "Inherent self-interference cancellation at 900 mhz for in-band full-duplex applications," in *2018 IEEE 19th Wireless and Microwave Technology Conference (WAMICON)*. IEEE, 2018, pp. 1–4.
- [23] H. Soury and B. Smida, "Optimal pilot overhead for FDD full-duplex communication and radar sensing (consens)," in *IEEE Military Communications Conference (MILCOM)*. IEEE, 2017, pp. 725–730.
- [24] S. Khaledian, F. Farzami, B. Smida, and D. Erricolo, "A power-efficient implementation of in-band full-duplex communication system (ReflectFX)," in *International Symposium on Signal, Image, Video and Communications (ISIVC)*. IEEE, 2016, pp. 242–246.
- [25] M. Duarte, C. Dick, and A. Sabharwal, "Experiment-driven characterization of full-duplex wireless systems," *IEEE Transactions on Wireless Communications*, vol. 11, no. 12, pp. 4296–4307, Dec. 2012.
- [26] D. Korpi, M. Turunen, L. Anttila, and M. Valkama, "Modeling and cancellation of self-interference in full-duplex radio transceivers: Volterra series-based approach," in *2018 IEEE International Conference on Communications Workshops (ICC Workshops)*. IEEE, 2018, pp. 1–6.
- [27] B. Radunovic, D. Gunawardena, P. Key, A. Proutiere, N. Singh, V. Balan, and G. Dejean, "Rethinking indoor wireless mesh design: Low power, low frequency, full-duplex," in *IEEE Workshop on Wireless Mesh Networks (WIMESH 2010)*. IEEE, 2010, pp. 1–6.
- [28] M. Duarte and A. Sabharwal, "Full-duplex wireless communications using off-the-shelf radios: Feasibility and first results," in *Asilomar Conference on Signals, Systems and Computers (ACSSC)*. IEEE, 2010, pp. 1558–1562.
- [29] E. Everett, A. Sahai, and A. Sabharwal, "Passive self-interference suppression for full-duplex infrastructure nodes," *IEEE Transactions on Wireless Communications*, vol. 13, no. 2, pp. 680–694, 2014.
- [30] V. Syrjala, M. Valkama, L. Anttila, T. Riihonen, and D. Korpi, "Analysis of oscillator phase-noise effects on self-interference cancellation in full-duplex OFDM radio transceivers," *IEEE Transactions on Wireless Communications*, vol. 13, no. 6, pp. 2977–2990, 2014.
- [31] A. Masmoudi and T. Le-Ngoc, "Channel estimation and self-interference cancellation in full-duplex communication systems," *IEEE Transactions on Vehicular Technology*, vol. 66, no. 1, pp. 321–334, 2017.
- [32] A. Balatsoukas-Stimming, "Non-linear digital self-interference cancellation for in-band full-duplex radios using neural networks," in *2018 IEEE 19th International Workshop on Signal Processing Advances in Wireless Communications (SPAWC)*. IEEE, 2018, pp. 1–5.
- [33] H. Iimori, G. Abreu, and G. C. Alexandropoulos, "Full-duplex bi-directional MIMO under imperfect CSI and hardware impairments," in *2018 15th Workshop on Positioning, Navigation and Communications (WPNC)*. IEEE, 2018, pp. 1–6.
- [34] N. M. Gowda and A. Sabharwal, "JointNull: Combining partial analog cancellation with transmit beamforming for large-antenna full-duplex wireless systems," *IEEE Transactions on Wireless Communications*, vol. 17, no. 3, pp. 2094–2108, 2018.
- [35] Z. Li, Y. Xia, W. Pei, K. Wang, and D. P. Mandic, "An augmented nonlinear lms for digital self-interference cancellation in full-duplex direct-conversion transceivers," *IEEE Transactions on Signal Processing*, vol. 66, no. 15, pp. 4065–4078, 2018.
- [36] M. S. Sim, K. S. Kim, and C.-B. Chae, "Self-interference cancellation for LTE-compatible full-duplex systems," in *2018 IEEE International Conference on Communications Workshops (ICC Workshops)*. IEEE, 2018, pp. 1–6.
- [37] Q. Gu, *RF system design of transceivers for wireless communications*. Springer Science & Business Media, 2005.
- [38] T. Schenk, *RF imperfections in high-rate wireless systems: impact and digital compensation*. Springer Science & Business Media, 2008.
- [39] AD9361: 2×2 RF Agile Transceiver, Rev. F, Analog Devices, <http://www.analog.com/media/en/technical-documentation/data-sheets/AD9361.pdf>.